SPECTROSCOPIC TECHNIQUES FOR DETERMINING ELECTRON DENSITIES IN THE SOLAR ATMOSPHERE

H. Mason

JOURNAL DE PHYSIQUE
Colloque C1, Supplément au n°3, Tome 49, Mars 1988

SPECTROSCOPIC TECHNIQUES FOR DETERMINING ELECTRON DENSITIES IN THE SOLAR ATMOSPHERE

H.E. MASON

DAMTP, Silver Street, GB-Cambridge CB3 9EW, Great-Britain

ABSTRACT

The determination of electron density in the solar atmosphere using diagnostic line ratios has been a field of intense activity over the past ten years. These spectroscopic techniques have given us an insight into the physical conditions of such diverse phenomena as flares, active regions, sunspots, coronal holes and the quiet Sun. In this paper, an overview will be given of the methods used for determining electron densities in the solar atmosphere. This will include a discussion of the accuracy of the atomic parameters required in such analyses. Several different approximations are used to calculate electron scattering cross-sections. These will be outlined and their accuracy for individual ions will be assessed.

The use of these techniques have led to some fundamental discoveries about the nature of the solar atmosphere. The transition region was conventionally envisaged as a homogeneous layer between the low temperature chromosphere and the high temperature corona. We now know that the transition region has unresolved filamentary structures with very small "filling factors" at low temperatures. In contrast, the coronal emission seems to be more homogeneously distributed. A lot of effort has gone into the determination of the electron densites in solar flares, particularily during the impulsive phase. Such studies are crucial to distinguish between various theoretical flare models. These problems will be discussed in relation to analyses of spectral data from SKYLAB, HRTS, SMM, SOLEX and XSST and with a view to future projects such as SOHO.

1 SOLAR OBSERVATIONS

The visible surface of the sun (photosphere) has a characteristic temperature of 6000 °K. In contrast, the temperature of the corona is around 10^6 °K and there is a very steep temperature gradient in the transition region between the chromosphere and the corona (fig. 1). The mechanism for heating the corona is not understood and remains one of the fundamental questions in solar physics. Although initial models of the solar atmosphere were homogeneous and spherically symmetrical, it is now known that this is a gross over simplification. The structures in the outer atmosphere are determined by the magnetic field distribution. From X-ray pictures, one can distinguish various features such as active region loops, bright points and coronal holes. The redistribution of magnetic field configurations in active regions leads to explosive events called solar flares, where the temperatures exceed 10^7 K. High spatial resolution images of the transition region and chromospheric emission show small (1") filamentary structures protruding into the corona. The nature of these structures and of the overall transition region is not understood. To distinguish between various models for these and many other solar features, it is necessary to derive the pressure as a function of temperature. Spectroscopic electron density diagnostics provide that information.

Spectral line intensities can be used to determine the physical parameters of the plasma, such as abundance, electron and ion temperature and electron density. The line profiles provide information on turbulent broadening and flows. In fig. 2, the characteristic temperature of the emission lines is indicated as a function of wavelength. The highest temperature emission from solar flares falls predominantly in the X-ray wavelength region. Only a few high temperature lines are seen the UV wavelength, the strongest flare line above 1000Å being the Fe XXI line at 1354.1Å. The coronal and transition region emission is spread across a wavelength region from 150-1300Å. The chromospheric emission falls predominantly at longer wavelengths. Overlayed on this illustration, is a summary of the principal satellites launched from the USA since 1969, which have carried spectroscopic instruments. Rocket flights are not listed, with the exception of XSST. It should be noted that the HRTS instrument was flown several times on rockets before the Spacelab II mission. The recent Japanese satellite, Hinatori, is include for reference. It would be impossible to summarise all the results from the analyses of these spectra. Excellent reviews are given in the books published as a result of the workshop series for OSO, Skylab, SMM and Hinatori.

The scope for this presentation is enormous, so it will be necessary to restrict the areas covered. Reference will be given to three previous reviews in this field (Dere and Mason, 1981, Gabriel and Mason, 1982, Doschek, 1985). In those papers, details were given of the various methods for determining electron density and analyses of available solar data were reviewed. In this paper, recent anayses of solar spectra have been selected to illustrate the diagnostic techniques and an assessment is presented of the atomic parameters used in such analyses.

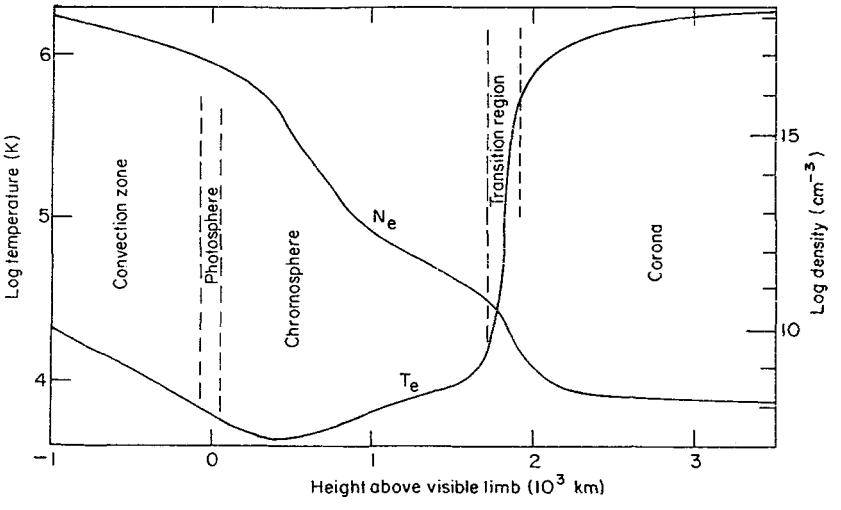

Fig. 1 Schematic representation of the variation with height of the mean values of temperature and density in the outer layers of the sun. Gabriel and Mason (1982)

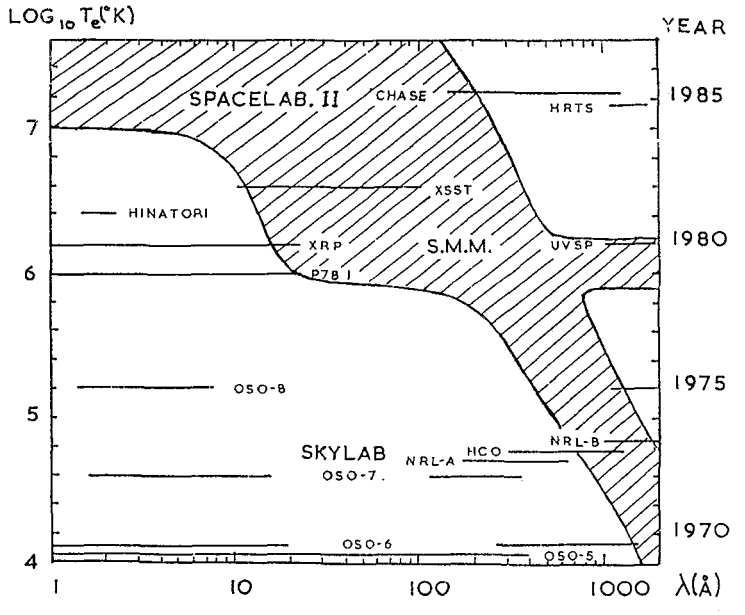

Fig. 2 Schematic illustration of the distribution of the characteristic temperature of the spectral emission lines as a function of λ(Å). Superimposed on this are the solar satellites launched in the USA.

2 ATOMIC PARAMETERS

2.1 Line emissivity

The line emissivity (per unit volume, per unit time) is

$$\varepsilon(\lambda_{ij}) = N_j A_{ji} h c / \lambda_{ij} \qquad (j > i)$$

where A_{ji} is the spontaneous radiative transition probability and N_j is the number density of level i.

$$N_j = \frac{N_j(X^{+m})}{N(X^{+m})} \quad \frac{N(X^{+m})}{N(X)} \quad \frac{N(X)}{N(H)} \quad \frac{N(H)}{N_e} \quad N_e$$

where N_e is the electron number density, $N(H)/N_e$ is the Hydrogen abundance, $N(X)/N(H)$ is the element abundance, $N(X^{+m})/N(X)$ is the ionisation ratio of the ion X^{+m} relative to the total number desity of element X (function of T_e) and $N_j(X^{+m})/N(X^{+m})$ is the population of level j relative to the total number density of the ion X^{+m} (function of N_e, T_e). The total spectral line intensity is then:

$$I(\lambda_{ij}) = \int_V \varepsilon(\lambda_{ij})\, dV$$

For a simple two level ion in 'coronal equilibrium', the excited level, j, is populated by electron collisional excitation from the ground level, i, and depopulated by spontaneous radiative decay.

$$N_i N_e C_{ij} = N_j A_{ji}$$

The electron collisonal excitation rate is obtained by integrating the electron collision cross-section over a Maxwellian velocity distribution:

$$C_{ij} = 8.63\times10^{-6}\ \Upsilon\ \exp[-\Delta E_{ij}/kT_e]\ /(\omega_i T_e^{1/2})$$

where Υ is an 'averaged' electron collision strength.For 'coronal eqilibrium, the population of the excited levels is much less than that of the ground level. The line emissivity can be re-written as :

$$\varepsilon(\lambda_{ij}) = \frac{N_i}{N}\frac{N(X^m)}{N(X)}\frac{N(X)}{N(H)}\frac{N(H)}{N_e} C_{ij}\frac{hc}{\lambda_{ij}} N_e^2$$

$$I(\lambda_{ij}) = \int_V G(T_e)\ N_e^2\ dV$$

For some 'forbidden' or 'intersystem' transitions, the radiative decay rate is so small that the electron collisions compete as a depopulating mechanism. The population of the emitting or 'metastable' level can become comparible with that of the ground level. It is the presence of such metastable levels which provides density diagnostic line ratios. Spectral emission lines can be grouped into three categories :

(i) 'allowed' lines $I \propto N_e^2$

(ii) 'forbidden' or 'intersystem' levels which originate in metastable levels

$I \propto N_e^2$		low N_e
$I \propto N_e^\beta$	$(1<\beta<2)$	intermediate N_e
$I \propto N_e$		high N_e

(iii) 'allowed' lines which are excited from metastable levels

$I \propto N_e^2$		low N_e
$I \propto N_e^\gamma$	$(2<\gamma<3)$	intermediate N_e
$I \propto N_e^2$		high N_e

In the discussion above, the models are simplified. In actual calculations, it is necessary to solve the statistical equilibrium equations for many levels in each ion, taking account of all the various excitation and de-excitation processes.

2.2 Atomic structure calculations

In atomic structure calculations, the wavefunctions are often expanded in terms of Slater states (eg SSTRUCT, Eissner et al, 1974). The radial equations for the individual electrons are solved using a scaled central field potential ($V_{nl}(r)$; Z/r, $r\to0$; $(Z-N+1)/r$, $r\to\infty$). The diagonalisation of the energy matrix for the total wavefunction determines the 'configuration mixing' coefficients. To obtain accurate wavefunctions for highly ionised systems, it is necessary to include all configurations in the same complex (same principal quantum number and parity). It is essential to chose an optimum set of configurations. The atomic structure calculations can be improved using various techniques. Neglected configurations can be represented by 'pseudo' states. Semi-empirical fitting procedures can be used with the observed energy levels. For really accurate results, the techniques of collision theory can be used to solve the bound state problem. For highly ionised systems such as those occuring in the solar corona it is necessary to transform LS coupling results into intermediate coupling taking account of relativistic corrections to the Hamiltonian. For very heavy ions ($Z \geqslant 30$) it is necessary to carry out full relativistic calculations. The accuracy obtained for atomic most atomic structure calculations is very high and radiative transition probabilities can be calculated to better than 10%.

2.3 Electron scattering calculations

The 'distorted wave' (DW) approximation neglects the coupling of the channels (target state + scattering electron). The scattering electron sees a central field potential. The DW approximation is therefore only valid for systems which are a few times ionised. Exchange contributions can be included. The program DISTWAV (Eissner and Seaton,1972) has been extensively used by Mason and co-workers for ions of solar interest. The accuracy of the collision strengths is generally assumed to be about 25%. For high partial wave values, the Coulomb Bethe (BETHE) approximation can be used. In this approximation it is assumed that the scattering electron does not penetrate the target. For dipole transitions:

$$\Omega^{a} = \frac{4\pi\ \omega_i\ f_{ij}\ g}{3\qquad \Delta E_{ij}}$$

In this formula, the Gaunt factor, g, is calculated using Coulomb wave functions. Often, a semi-empirical scaling factor, $\bar{g}$ is substituted. This $\bar{g}$ method of obtaining collision strengths should be used no other calculations are available.

In the 'close coupling' approximations, the scattering electron 'sees' individual target electrons, the channels are coupled and a set of integro-differential equations are solved. Two sets of close coupling codes have been used extensively for astrophysical ions : IMPACT (Crees et al, 1978) and RMATX (Berrington et al.,1978). Close coupling calculations are expensive, and it has often been necessary to severely truncate the number of target terms included. Neglected long range target states and continuum states are often represented by 'pseudo' states. The resonance contribution to the electron excitation rate can be extremely important especially for forbidden and intersystem transitions. Close coupling results should in general be accurate to better than 10%.

A detailed comparison between the various methods has been carried out by Burgess et al (1987a, 1987b) for the allowed transitions of MgX and MgVII. For MgVII, a substantial discrepancy ($\sim$45%) was found by Aggarwal (1985) between his close coupling calculations (RMATX) and the previously published DISTWAV values of Mason and Bhatia (1978). The targets used in the two publications were very different, Aggarwal's target was much more elaborate. Burgess et al (1987b) have taken a simple three configuration target and run the various computer codes DISTWAV, IMPACT, RMATX, CBETHE. Burgess et al find excellent agreement (2%) between the close coupling and DW calculations . It appears that Aggarwal used an incorrect treatment for the asymptotic region leading to an underestimation of the collision strengths. He used RMATX(COUL) beyond a boundary radius of 3.5au and did not take correct account of the long range potential. This problem only arises for dipole transitions.

Several atomic data banks are being compiled around the world. The atomic data are usually stored as raw data (eg R-matrices or collision strengths). A couple of useful compilations of electron scattering data have recently been published by Gallagher and Pradhan (1986) and Eissner (1987). What the astrophysicist requires is easily accessible, processed and assessed atomic data. Burgess and Tully (1987) have recently developed a method of processing raw data in the graphical form . This method is being used to compile a compact databank for input into astrophysical codes such as emission measure and transient ionisation codes.

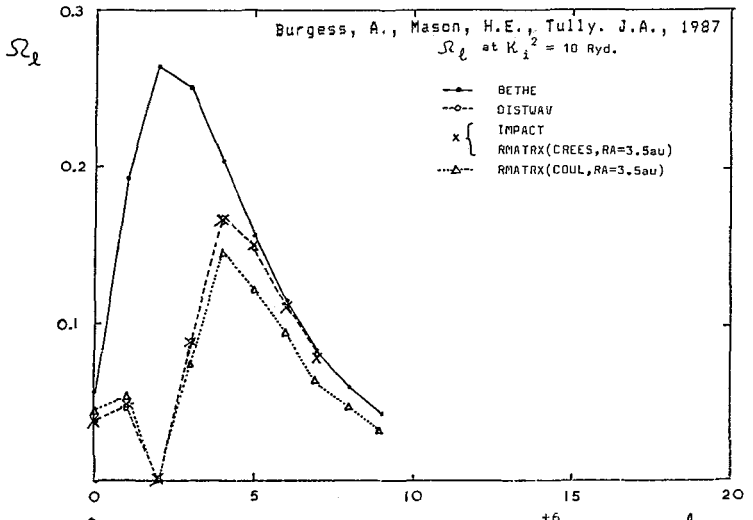

Figure 3 Partial Electron Collision Strengths for Mg^{+6}
Transition $2s^2 2p^2\ ^1S - 2s2p^3\ ^1P$

3 SPECTROSCOPIC DIAGNOSTICS

3.1 Helium Like Ions

Gabriel and Jordan (1969) proposed that the line intensity R of the forbidden (F, $1s^2\ ^1S_0$ - $1s2s\ ^3S_1$) line to the intercombination (I, $1s^2\ ^1S_0$ - $1s2p\ ^3P_1$) line from the Helium like ions would be a good electron density diagnostic for solar plasmas. For low densities, the excited levels are populated from the ground state by electron collisions and decay by radiative transitions. As the density increases, electron collisions cause transitions from $1s2s\ ^3S$ to $1s2p\ ^3P$, decreasing the ratio R below it's low density limit. A number of refined calculations have been carried out for the Helium like ions. Recommended atomic data are given by Nakazaki and Kato (1987). The first observation of a large variation in R was reported by McKenzie et al. (1980a) from the p78-1 solar flare observations of the OVII lines. Their results are reproduced in fig. 4, the electron density was found to exceed 10^{11} cm^{-3} during the flare maximum. High time resolution spectra of other flares show a strong, short lived density enhancement ($N_e > 10^{12}$ cm^{-3}) coincident with the peak in the hard X-ray emission (Doschek et al, 1981). The temperature of maximum abundance for OVII is 2×10^6 K, which is characteristic of the solar corona. The authors gave two possible interpretations for these results : the first is that a compression of the plasma enhances the electron density, the second is that successively deeper and denser layers of the solar atmosphere are heated during the solar flare. Electron density measurements have also been derived from the ratio R for the Helium like ion NeIX recorded by the SMM-XRP-FCS instrument (Woolfson et al, 1983). McKenzie (1985) pointed out the posibility of contamination by FeXIX lines which also fall in this wavelength region. Detailed calculations confirm that when the flare temperature is high ($\sim 10^7$ K), the contribution from the FeXIX lines to the NeIX lines can be significant (Bhatia et al, 1987). Several Helium like lines and other electron density sensitive line ratios fall into the wavelength region (10 - 100 Å) covered by the XSST instrument. Electron density diagnostics in this wavelength region were recently reviewed by Brown et al (1986). Results for a spectra obtained during the decay phase of a flare are given in fig. 5. Constant electron density, rather than constant pressure indicates that the structure of the flare is complex.

3.2 Highly Ionised Iron Ions

In recent year, SMM, P78-1 and Hinatori satellites have provided a wealth of solar flare spectra in the X-ray wavelength region. The diagnostic potential of the satellite lines and inner shell transitions has been fervently persued. The FeXVII - FeXXIV ions give rise to lines in the 10 - 20Å region (P78-1, McKenzie et al., 1980b and SMM-XRP-FCS, Phillips et al. ,1984) and in the 100-150Å region (OSO-5, Kastner et al., 1974). The diagnostic potential of the latter wavelength region was explored by Mason et al. (1984) and an electron density 4 x 10^{11} cm^{-3} was derived. It is a pity that this particular wavelength region has been so neglected since it is rich in solar flare lines. Tokamak spectra (Stratton et al,1984, Masai and Kato, 1986) have verified the intensity ratios predicted by Bhatia, Mason and co-workers for the higher electron densities obtained in the laboratory. This confirms that the DW approximation is reliable for these ions.

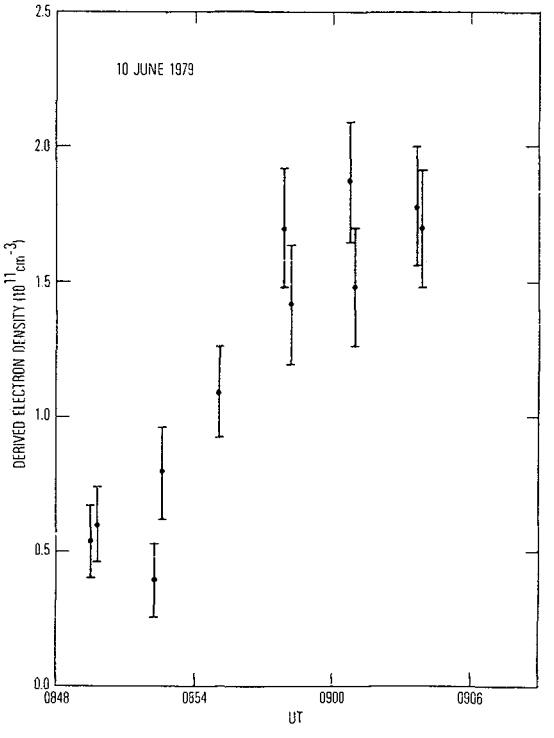

Fig. 4 The electron density of the flare plasma from which the O VII lines are emitted plotted as a function of time.
McKenzie et al (1980a)

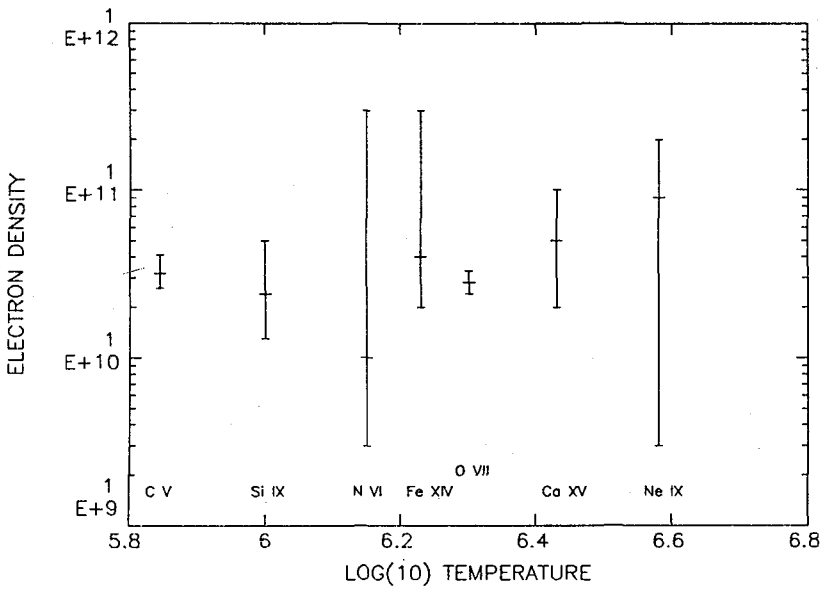

Fig. 5 Observed electron densities and error bars for seven diagnostic line pairs for a flare spectrum recorded by XSST. Brown et al. (1986)

3.3 Electron Density Diagnostics in the UV Wavelength Region

Electron density diagnostics for solar flares and active regions in the UV wavelength region were reviewed by Dere and Mason (1982) and Doschek (1985). Dere et al. (1979) studied the Skylab ATM-NRL-S082A spectroheliograms (170-630Å). These observations provide a valuable combination of spectra with images. These data are particularily appropriate to the study of compact flares. Several such flares have been studied. A recent paper by Widing and Cook (1987) combines electron density diagnostic ratios from this wavelength region with those from the longer wavelength region (1000-2000Å) to provide an electron density profile for the temperature range 5 x 10^4 to 10^7K (fig. 6).

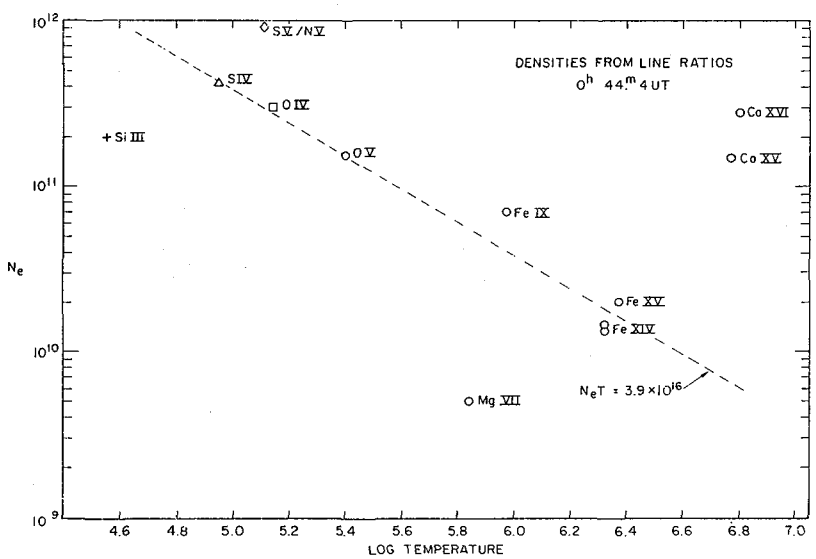

Fig. 6 Electron densities for a solar flare obtained using lines from ATM-NRL-A and NRL-B spectra. Widing and Cheng (1987).

These authors find that the emission from different temperatures is coming from different structures within the flare. In particular, the pressure at 5 x 10^6 K is more than an order of magnitude greater than that at lower temperatures (10^5 - 2 x 10^6 K). The high temperature loops appear to be embedded in a more diffuse region of low temperature emission. The low temperature emission does not seem to be confined to the footpoints of high temperature loops as some models predict.

The transition region diagnostics in the 1000-2000Å wavelength region fall into basically two categories: the ratio of lines from the same ion within a multiplet or the ratio of an intersystem line to an allowed line. In the latter method it is often necessary to to use different ions formed over a similar temperature range. In the first method, the intensity ratio changes very little over a large density range, so uncertainties in the atomic data or observed intensities can lead to large errors in the derived densities. It is essential to use accurate atomic scattering calculations, taking full account of the resonance contribution to the excitation rates. The ratio of the intersystem to the allowed transition varies rapidly and provides a sensitive method for determining the electron density. Unfortunately, uncertainties can arise in the analyses due to the difference in the emission functions for the lines involved and some of the intensity ratios are temperature dependent. An ion which has been extensively studied in the quiet Sun and active regions is CIII. Work on this ion is reviewed in Doschek (1985). More recently, interest has focussed on the OIV transitions $2s^22p\ ^2P$ - $2s2p^2\ ^4P$ which fall at around 1400Å. The intensity ratios of the spectral lines within the multiplet are density sensitive and have been extensively studied using Skylab ATM-NRL-S082B and HRTS spectra. The ratio of one of these lines to the SiIV 1402.77Å allowed line has also been used to determine electron density. The OIV ion has a maximum abundance at 1.7 x 10^5 K whereas the SiIV ion has a maximum abundance at 6 x 10^4 K. The ratio OIV/SiIV has recently been extensively studied using the SMM-UVSP instrument. High time resolution observations of the this ratio indicate that electron density enhancements of more than an order of magnitude are correlated with hard X-ray bursts during solar flares (Cheng et al.,1981, Cheng and Tandberg-Hanseen,1986). These results can be interpreted as the accelaration of high energy electrons in loop structures down into the footpoints. The interaction of the high energy electrons with the deeper atmosphere produces hard X-ray emission and heats the dense low temperature plasma (10^4 K) to 10^5 K, producing the UV brightenings. The UV brightenings are not confined to

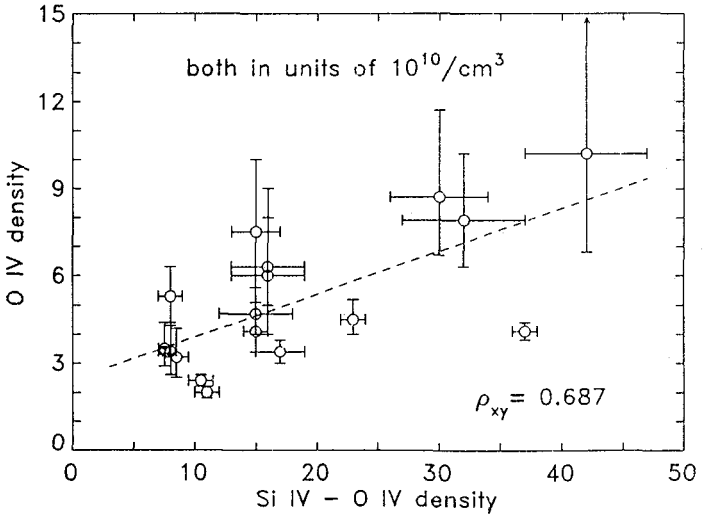

Fig. 7 Comparison of the electron densities derived from the Si IV/O IV diagnostic with those from the O IV multiplet only. Hayes and Shine (1987).

solar flares. The transition region shows the existence of continual small scale activity. Hayes and Shine (1987) studied the characteristics of these bursts. They also compared the two methods for determining electron density discussed above. Fig. 7 shows the density derived from the OIV multiplet compared to the density derived from the SiIV/OIV ratio. The inconsistency between the two methods could be due to the effect of small dense structures embedded in a background transition region as predicted by Doshek (1984). The emission from the forbidden lines is weigted as N_e, whereas the emission from the allowed transition is weighted as N_e^2. The density measurements from these diagnostics must therefore be considered as an average from different emission regions. An alternative explanation for the discrepancy between the derived densities could be due to the assumptions made about the emission measure distribution. This important aspect of density diagnostic techniques should be persued in order to understand the nature of these UV bursts.

The electron density diagnostics in the UV wavelength region were summarised by Dere and Mason (1981)(fig. 8). A summary of the electron pressure values obtained for different regions is summarised in table I taken from Doschek (1985). "Filling factors" for the transition region emission are extremely small (0.1-0.001)(Dere,1982). Feldman (1983) discussed the implications of the transition region observations. He suggested that the transition region emission comes from two emitting regions: the "classical" transition region between the chromosphere and corona and unresolved filamentary structures extending into the corona (10") whose nature is at present unknown.

This wavelength region will be covered by spectroscopic instruments on SOHO. These instruments will combine high spatial, spectral and temporal observations of the solar atmosphere and will address some fundamental questions about the heating mechanism for the solar corona, and the origin of the solar wind. Diagnostic techniques for determining the physical parameters in the different solar features will play an important role in the operation of the instruments on SOHO.

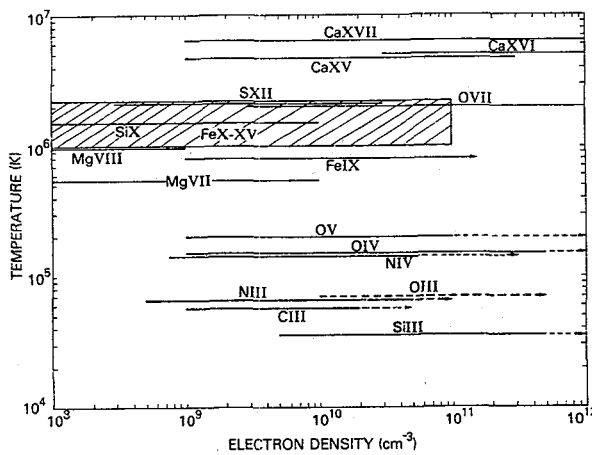

Fig. 8 Range of density sensitive lines formed at different temperatures Dere and Mason (1981)

TABLE I
Electron Pressures

Region	Log ($N_e T_e$)
Quiet sun (chromosphere)	15.2
Quiet sun (transition region)	15.1
Quiet sun (corona)	15.0 ($h > 20$ arc-sec)
Coronal hole (transition region)	15.1 (14.8)
Active region (chromosphere)	15.2
Active region (transition region)	15.9
Active region (corona)	15.2–16.0
Prominence (transition region)	14.9
Sunspot (transition region)	15.0
Surges (flare-related activity) (transition region)	15.0–16.2
Flares (transition region)	16.0–18.0
Flares (coronas, 10^6 K < T_e < 6×10^6 K)	16.8–18.7

References

Aggarwal, K.M., 1985, Ap.J., 58, 289
Berrington, K.A., Burke, P.G., LeDourneuf, M., Robb, W.D., Taylor, T.K., Vo Ky Lan, 1978, Comp. Phys. Comm., 14, 367
Bhatia, A.K., Lemen, J.R., Mason, H.E., Phillips, K.J.H., 1987, preprint
Brown, W.A., Mason, H.E., Brunner, M.E., Acton, L.W., 1986, Ap.J..301,981
Burgess, A., Mason, H.E., Tully. J.A., 1987, preprint
Burgess, A., Tully, J.A., 1987, preprint
Cheng, C.C. and Tandberg-Hanssen, E., 1986, Ap. J., 309, 421

Cheng, C.C., Tandberg-Hanssen, E., Brunner, E.C., Orwig, L., Frost, K.J., Kenny, P.J., Woodgate, B.E., Shine, R.A., 1981, Ap.J., 248, L39
Crees, M., Seaton, M.J.S. and Wilson, P., 1978, Comp. Phys. Comm., 15, 23
Dere, K.P., 1982, Sol. Phys., 75, 189
Dere, K.P. and Mason, H.E., 1981, Ch. 6, 'Active Regions', ed. F.Orrall
Dere, K.P., Mason, H.E., Widing, K.G., Bhatia, A.K., Ap.J. Suppl, 40, 341
Doschek, G.A., 1984, Ap.J., 279, 446
Doschek, G.A., 1985, Ch. 6, 'Autoionisation', ed. A. Tempkin
Doschek, G.A., Feldman, U., Landecker, P.B., McKenzie, D.L., 1981, Ap.J., 249,372
Eissner, W., 1986, 'Atomic Data Workshop', DL/SCI/R24
Eissner, W., Jones, M., Nussbaumer, H., 1974, Comp. Phys. Comm., 8,270
Eissner, W. and Seaton, M.J., 1972, J.Phys.B, 5, 2187
Feldman, U., 1983, Ap.J., 275, 367
Feldman, U., Doschek, G.A., Rosenberg, F.D., 1977, Ap.J., 215, 652
Gabriel, A.H. and Jordan, C., 1969, Mon.Not.R.astr.Soc., 145, 241
Gabriel,A.H. and Mason,H.E., 1982,Ch.12,'Applied atomic collision Physics' Vol I, eds. H.S.W. Massey, B. Benderson, E.W. McDaniel
Gallagher, J.W. and Pradhan, A.K., 1985, JILA Rep #30
Hayes, M and Shine, R.A., 1987,AP.J., 312, 943
Kastner, S.O., Neupert, W.M., Swartz, M, 1974, Ap.J., 191, 26
Masai, K. and Kato, T., 1986, Rep # IPPJ 787
Mason, H.E., Bhatia, A.K., Kastner, S.O., Neupert. W.M., Swartz, M., Sol. Phys., 92, 199
McKenzie, D.L., Broussard, R.M., Landecker, P.B., Rugge, H.R., Young, R.M. Doschek, G.A., Feldman, U., 1980a, Ap.J., 238, L43
McKenzie, D.L., Broussard, R.M., Landecker, P.B., Doschek, G.A., Feldman, U., 1980b, Ap.J., 241, 409
Nakasaki, S. and Kato, T., 1987, pre-print
Phillips, K.J.H., Leibacher, J.W., Wolfson, C.J., Fawcett, B.C., Kent, B.J., Mason, H.E., Acton, L.W., Culhane, J.L., Gabriel, A.H. Ap.J., 256, 774
Stratton, B.C., Moos, H.W., Finkenthal, M., 1984, Ap.J., 279, L31
Widing, K.G. and Cheng, C.C., 1987, Ap.J., in press
Wolfson, C.J., Doyle, J.G., Leibacher, J.W., Phillips, K.J.H., 1983, Ap.J., 269, 319